

ConvRot: Rotation-Based Plug-and-Play 4-bit Quantization for Diffusion Transformers

Feice Huang^{1†*}, Zuliang Han^{2*}, Xing Zhou², Yihuang Chen², Lifei Zhu², Haoqian Wang^{1‡}
¹SIGS, Tsinghua University ²Central Media Technology Institute, Huawei

Abstract

Diffusion transformers have demonstrated strong capabilities in generating high-quality images. However, as model size increases, the growing memory footprint and inference latency pose significant challenges for practical deployment. Recent studies in large language models (LLMs) show that rotation-based techniques can smooth outliers and enable 4-bit quantization, but these approaches often incur substantial overhead and struggle with row-wise outliers in diffusion transformers. To address these challenges, we propose ConvRot, a group-wise rotation-based quantization method that leverages regular Hadamard transform (RHT) to suppress both row-wise and column-wise outliers while reducing complexity from quadratic to linear. Building on this, we design ConvLinear4bit, a plug-and-play module that integrates rotation, quantization, GEMM, and dequantization, enabling W4A4 inference without retraining and preserving visual quality. Experiments on FLUX.1-dev demonstrate a $2.26\times$ speedup and $4.05\times$ memory reduction while maintaining image fidelity. To our knowledge, this is the first application of rotation-based quantization for plug-and-play W4A4 inference in diffusion transformers.

1. Introduction

Diffusion models generate high-fidelity images [9, 24], but scaling their architectures significantly increases memory and inference costs. The recently released Qwen-Image model [30] reaches a scale of 20B parameters, requiring more than 60 GiB of GPU memory for inference. Quantization is widely used in LLMs to reduce model size and improve inference speed [4, 31, 37], mainly by reducing memory movement and leveraging low-precision compute units in modern GPUs. This makes quantization a promising direction for reducing the memory and latency cost of diffusion models as well. A major source of accuracy loss in quantization comes from outliers, which can distort the

scaling factors and degrade performance. Recent studies in LLMs show that rotation-based quantization methods redistribute outliers across channels, enabling 4-bit quantization with minimal accuracy loss [2, 17, 28], but the extra rotation operations bring non-negligible overhead that offsets part of the speedup. Therefore, the key challenge is to apply rotation-based quantization to diffusion transformers while preserving accuracy and minimizing rotation overhead.

As illustrated in Figure 1, rotation-based quantization methods suppress outliers by applying rotational transformations to both weights and activations. While these methods have been extensively studied in LLMs, directly applying them to diffusion models faces two major challenges. First, the rotation operations themselves introduce substantial computational overhead. Prior works attempt to mitigate this using techniques such as the Fast Walsh-Hadamard Transform (FWHT), which is equivalent to multiplying by Sylvester-type Hadamard matrices, thereby limiting the choice of rotation matrices. They also leverage operation fusion to reduce the need for online rotations [2]. However, the Adaptive LayerNorm (AdaLN) design in Diffusion Transformers (DiTs) [22] can break these fusion strategies, forcing additional online rotations and offsetting the acceleration benefits. Sparse rotation matrices have also been explored [14], but without efficient low-level support, they do not lead to practical speedup. Second, as shown in Figure 3, we observe row-wise outliers in certain layers of FLUX.1-dev [3], which differs from the column-wise outlier patterns com-

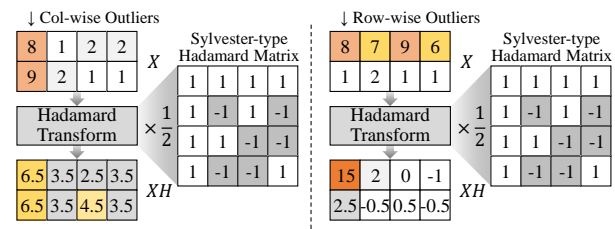


Figure 1. Rotation-based quantization methods using Hadamard matrices can effectively suppress outliers by redistributing energy across channels. However, Sylvester-type Hadamard matrices lead to energy concentration when encountering row-wise outliers.

[†]Work done during an internship at Central Media Technology Institute.

*Equal contribution. [‡]Corresponding author.

monly found in LLMs. Existing rotation matrix designs, particularly Hadamard matrix-based methods, primarily target column-wise outliers and are therefore ineffective at handling row-wise outliers, leading to noticeable accuracy degradation. Recent work [6] also observed that applying Hadamard directly to DiT can cause degradation due to mean and scale differences across channels.

In this work, we propose ConvRot, a novel rotation-based quantization paradigm. First, we introduce a group-wise rotation scheme that reduces computational complexity from $\mathcal{O}(K^2)$ to $\mathcal{O}(K)$, where K is the number of channels, and allows flexible trade-offs between computation cost and outlier suppression by adjusting the group size N_0 . Second, we adopt the regular Hadamard Transform (RHT) to simultaneously suppress row-wise and column-wise outliers. To support this, we propose a theoretical framework: we formalize the column sum squared property of Hadamard matrices, define the column discrepancy to quantify imbalance, and present a Kronecker-based construction of regular Hadamard matrices for orders that are powers of four, guaranteeing minimal column discrepancy. Based on these regular Hadamard matrices, we implement group-wise RHT with a conv-like matmul operation on weights and activations, which we name ConvRot. Finally, we design ConvLinear4bit, a plug-and-play module that integrates rotation, quantization, GEMM, and dequantization, avoiding expensive loops or extra memory movement while leveraging mature matrix multiplication pipelines on modern GPUs, without requiring complex operator design or additional inference engines. Experimental results demonstrate that ConvRot largely preserves image quality, reduces the memory footprint of the original BF16 DiT by $4.05\times$, and achieves a $2.26\times$ speedup on an RTX 4090 24GB.

In summary, our main contributions are:

- We provide a theoretical framework for rotation-based quantization: we define the column discrepancy to quantify column sum imbalance, and propose a Kronecker-based construction of regular Hadamard matrices for orders that are powers of four, guaranteeing minimal column discrepancy and therefore particularly effective at mitigating the amplification of row-wise outliers in activations.
- We propose ConvRot, a novel group-wise rotation-based quantization paradigm that leverages regular Hadamard Transform (RHT) to simultaneously smooth row-wise and column-wise outliers, reducing computational complexity from $\mathcal{O}(N^2)$ to $\mathcal{O}(N)$ and significantly lowering latency compared to global rotations.
- We design ConvLinear4bit, a plug-and-play module that integrates rotation, quantization, GEMM, and dequantization, enabling training-free W4A4 inference for all linear layers in diffusion models.
- To the best of our knowledge, we are the first to achieve training-free, fully 4-bit (W4A4) inference on diffusion

transformers with acceptable accuracy degradation, without auxiliary high-precision branches and while avoiding major visual artifacts.

2. Related Work

2.1. Quantization for LLMs

Quantization reduces memory traffic and computation by adopting low-precision formats, while also enabling efficient use of hardware-specific accelerators such as INT4 tensor cores [4, 7, 15]. However, naive per-tensor or per-channel post-training quantization (PTQ) schemes suffer from outliers that dominate the dynamic range, leading to substantial accuracy degradation. Rotation-based quantization addresses this by applying orthogonal transforms to distribute outliers across channels, producing smoother distributions with fewer extreme values [28]. Yet, these rotations introduce quadratic complexity, which offsets the potential acceleration. Prior works mitigate the cost with fast hadamard transforms [2], fuse the rotation into adjacent linear layers [17], or block-diagonal rotations [14]. While effective for LLMs, these designs face challenges in diffusion models, fusion breaks under adaptive normalization layers [22], and block-diagonal rotations fail to deliver speedup proportional to their reduced computation. In contrast, our ConvRot employs a lightweight group-wise rotation that reduces complexity to linear while preserving sufficient smoothing, and can be directly applied to diffusion models without architectural changes.

2.2. Acceleration of Diffusion Models

Diffusion models [9] achieve state-of-the-art performance in image and video generation [10, 30], but their inference speed remains a major limitation for deployment due to the inherently slow and computationally intensive iterative process. Existing acceleration strategies include few-step sam-

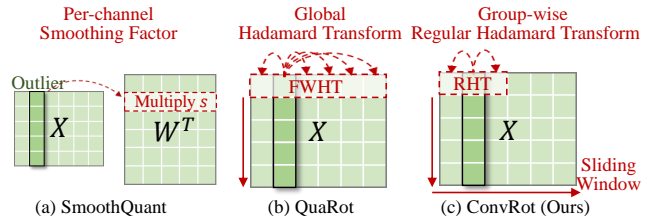


Figure 2. Illustration of how different transformations redistribute outliers. (a) **SmoothQuant** [31]: per-channel diagonal transform $T(\mathbf{X}) = \mathbf{X} \text{ diag}(\mathbf{s})^{-1}$ shifts activation outlier magnitudes into the corresponding channel weights. (b) **QuaRot** [2]: global Hadamard transform $T(\mathbf{X}) = \mathbf{X}\mathbf{H}$ with orthogonal \mathbf{H} evenly redistributes activation energy. (c) **ConvRot (Ours)**: Group-wise Regular Hadamard Transform performs local smoothing of activations within sliding windows.

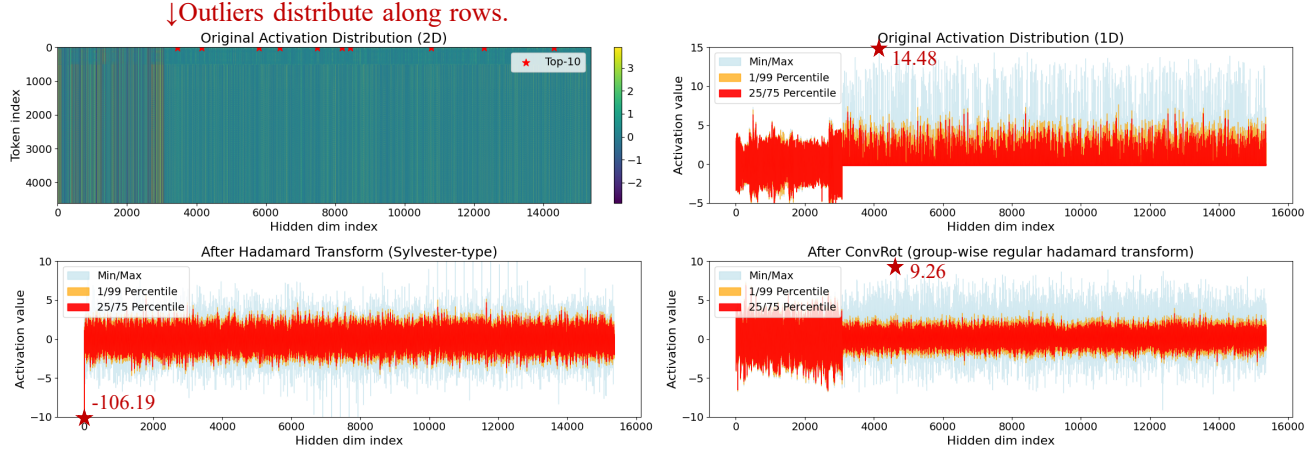


Figure 3. Effect of Hadamard transforms on the `single_transformer_blocks.37.proj_out` activations in Flux. The standard transform amplifies outliers ($\max = 106.19$), while the group-wise regular transform suppresses them ($\max = 9.26$), compared to the original ($\max = 14.48$).

plers [18, 19, 26], distillation [20, 25, 33], pruning [36], and caching [16]. Recently, quantization has also been explored for diffusion models [12, 13, 34, 35]. However, unlike language models, where latency is often dominated by weight loading, diffusion models are computationally bounded [12]. As a result, weight-only quantization is insufficient for diffusion models, both weights and activations must be quantized to fully exploit low-precision hardware. However, existing methods either maintain activations in higher precision [5], preventing the use of low-precision tensor cores, or rely on customized inference engines [12], which complicates deployment. By contrast, our method supports end-to-end 4-bit weight-activation quantization, fully exploiting low-precision hardware units. Furthermore, the proposed ConvLinear4bit layer is plug-and-play, requiring no specialized inference engine, and integrates seamlessly with existing quantized operators to deliver both memory reduction and practical speedup.

3. Preliminary

3.1. Equivalent Transformation Based Quantization Methods

Given an activation vector $\mathbf{x} \in \mathbb{R}^n$, a uniform b -bit quantizer is defined as

$$Q(\mathbf{x}) = \text{round}\left(\frac{\mathbf{x}}{s}\right), \quad (1)$$

where s is a scaling factor. Large-magnitude outliers in \mathbf{x} inflate s , reducing the effective resolution for most elements and making low-bit quantization challenging.

Transformation-based quantization methods apply an orthogonal or diagonal transformation $T(\cdot)$ to redistribute activation magnitudes before quantization while preserving the

computation. For a linear layer $\mathbf{Y} = \mathbf{X}\mathbf{W}^\top$, this invariance is expressed as

$$\mathbf{X}\mathbf{W}^\top = T(\mathbf{X})T'(\mathbf{W})^\top, \quad (2)$$

where $T'(\cdot)$ is the corresponding transform on the weight. As illustrated in Figure 2, different choices of $T(\cdot)$ correspond to different ways of redistributing outliers. The core challenge is to design $T(\cdot)$ to **suppress outlier amplitudes with minimal computational overhead**, enabling smaller scaling factors s and higher effective precision in low-bit quantization.

3.2. Regular Hadamard Matrix for Rotation

Definition 3.1 (Hadamard Matrix (\mathcal{H} -Matrix)). A Hadamard matrix (abbrev. \mathcal{H} -Matrix) $\mathbf{H}_n \in \{\pm 1\}^{n \times n}$ satisfies

$$\mathbf{H}_n \mathbf{H}_n^\top = n \mathbf{I}_n, \quad (3)$$

where \mathbf{I}_n is the $n \times n$ identity. Normalized by $1/\sqrt{n}$, \mathbf{H}_n is orthogonal, making it well-suited for rotation-based quantization since orthogonality redistributes outliers. Empirically, \mathcal{H} -Matrix rotations outperform random orthogonal ones [17, 28].

A common construction of Hadamard matrices is the Sylvester-type recursion, which produces a standard Hadamard matrix with the first row and column filled with 1s:

$$\mathbf{H}_1 = [1], \quad \mathbf{H}_{2n} = \begin{bmatrix} \mathbf{H}_n & \mathbf{H}_n \\ \mathbf{H}_n & -\mathbf{H}_n \end{bmatrix}.$$

The Fast Walsh-Hadamard Transform (FWHT) exploits this structure to reduce the matrix-vector multiplication complexity from $\mathcal{O}(n^2)$ to $\mathcal{O}(n \log n)$, using only additions and

subtractions. Recent work [14] demonstrates that block-wise rotations can preserve most of the benefits while reducing computational cost. It is worth noting that the FWHT is equivalent to multiplying by a Sylvester-type Hadamard matrix, *whose first column is all ones*, which can inadvertently amplify row-wise outliers in the activations, as illustrated in Figure 3.

Theorem 3.1 (Column Sum Squared Property). *For an \mathcal{H} -Matrix \mathbf{H}_n ,*

$$\sum_{j=1}^n \left(\sum_{i=1}^n \mathbf{H}_{ij} \right)^2 = n^2. \quad (4)$$

Definition 3.2 (Column Discrepancy). *For an \mathcal{H} -Matrix \mathbf{H}_n , the *column discrepancy* is defined as*

$$\|\mathbf{H}^\top \mathbf{1}\|_\infty = \max_j \left| \sum_i H_{ij} \right|, \quad (5)$$

where $\mathbf{1}$ is the all-ones vector. It measures the largest deviation of a column sum from zero.

This metric is related to *combinatorial discrepancy* [21, 27], defined for $A \in \{\pm 1\}^{n \times m}$ as

$$\text{disc}(A) = \min_{\varepsilon \in \{\pm 1\}^n} \|A^\top \varepsilon\|_\infty. \quad (6)$$

Here ε is a ± 1 coloring of rows, chosen to minimize the maximum column imbalance. In our case, the column discrepancy corresponds to the fixed coloring $\varepsilon = \mathbf{1}$, giving a natural upper bound on $\text{disc}(\mathbf{H})$.

For \mathcal{H} -Matrices, the column discrepancy always satisfies

$$\sqrt{n} \leq \|\mathbf{H}^\top \mathbf{1}\|_\infty \leq n. \quad (7)$$

The lower bound follows from the column sum squared property, while the upper bound is achieved by Sylvester-type matrices that contain identical columns. This motivates the study of *regular \mathcal{H} -Matrices*, which attain the minimum value.

Definition 3.3 (Regular \mathcal{H} -Matrix). *An \mathcal{H} -Matrix is *regular* if each row and column sums to $\pm \sqrt{n}$.*

Theorem 3.2. *Regular \mathcal{H} -Matrices attain the minimal possible column discrepancy:*

$$\max_j \left| \sum_{i=1}^n \mathbf{H}_{ij} \right| = \sqrt{n}. \quad (8)$$

Theorem 3.3 (Kronecker Construction). *For every $k \geq 1$, a regular \mathcal{H} -Matrix of order $n = 4^k$ exists. Starting from*

$$\mathbf{H}_4 = \begin{bmatrix} 1 & 1 & 1 & -1 \\ 1 & 1 & -1 & 1 \\ 1 & -1 & 1 & 1 \\ -1 & 1 & 1 & 1 \end{bmatrix}, \quad (9)$$

one obtains $\mathbf{H}_{4^{k+1}} = \mathbf{H}_{4^k} \otimes \mathbf{H}_4$ via the Kronecker product. Each \mathbf{H}_{4^k} remains regular.

All proofs are deferred to Appendix 7.

We leverage this property to design a *group-wise regular \mathcal{H} -Matrix rotation* scheme. It reduces peak activations and latency while preserving the smoothing benefits of \mathcal{H} -Matrix rotations, making it practical for large diffusion models where global rotations are expensive and may amplify outliers.

4. Method

In this work, we present an plug-and-play W4A4 quantization method for Diffusion Transformers (DiTs). As illustrated in Figure 4, Our approach consists of two core components: **ConvRot** and **ConvLinear4bit**. ConvRot performs group-wise regular Hadamard rotations, where the group-wise design reduces computational cost and the regular structure prevents row-wise outlier aggregation, smoothing activation and weight distributions before quantization. ConvLinear4bit integrates ConvRot, 4-bit quantization, matrix multiplication, and dequantization into a single linear layer, enabling straightforward plug-and-play replacement of the original layers. By simply replacing the original linear layers with ConvLinear4bit, we can perform low-precision inference on large-scale DiT models while maintaining high visual quality.

4.1. Motivation

Our first motivation comes from the high computational cost of existing rotation-based quantization methods, such as QuaRot [2] and SpinQuant [17], which typically apply a single global Hadamard rotation of order n . Because this approach redistributes outliers across all channels, it incurs quadratic complexity $\mathcal{O}(K^2)$, making it expensive for large-scale diffusion models. To reduce this cost, we propose limiting the rotation to smaller groups of size N_0 , allowing a flexible trade-off between computational overhead and the effectiveness of outlier smoothing.

The second motivation stems from a property of large Hadamard matrices with high-magnitude columns. As observed in FLUX (see Figure 3), when outliers in activations are distributed along specific rows, multiplying by such a matrix can inadvertently concentrate these outliers, increasing their magnitude instead of smoothing them. This row-wise aggregation arises mainly from the combination of large matrix size and column-sums with large absolute values. Applying Hadamard rotations on smaller, group-wise blocks alleviates this issue by limiting the rotation scope, while using regular Hadamard matrices further prevents the emergence of large-magnitude column-sums, effectively smoothing activations and avoiding outlier concentration.

These two insights motivate the design of ConvRot: (i) reducing computational cost by restricting the rotation scope, and (ii) preventing row-wise outlier concentration through the use of regular Hadamard matrices.

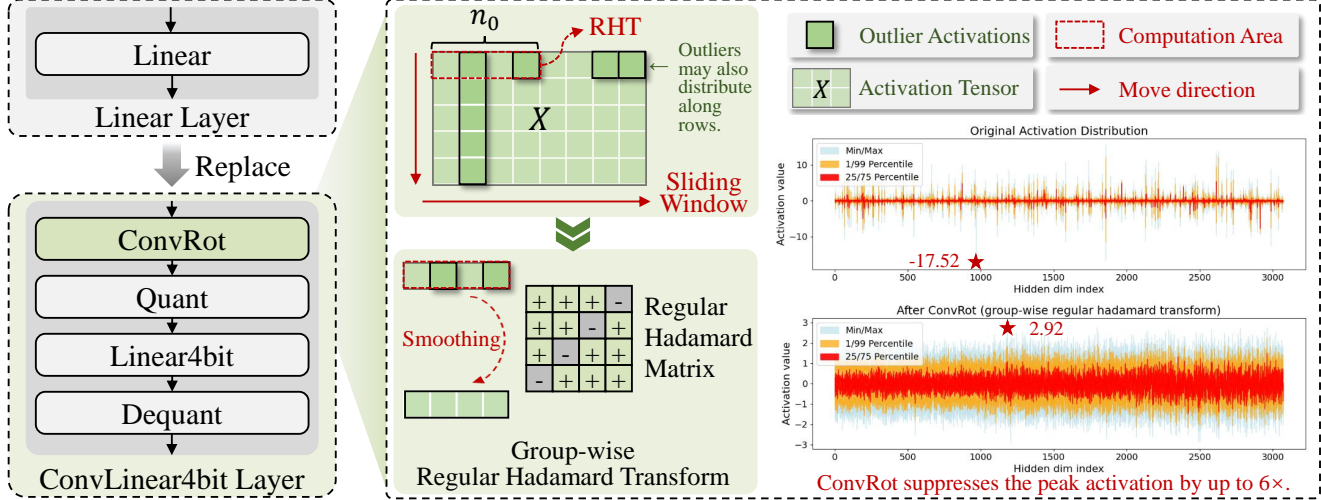


Figure 4. Overview of ConvRot. Left: ConvLinear4bit serves as a plug-and-play replacement for Linear layers. Right: ConvRot applies Regular Hadamard Transform (RHT) on non-overlapping sliding windows of the activation tensor, with each window multiplied by a regular Hadamard matrix.

4.2. ConvRot: Group-Wise Regular Hadamard Rotation

As discussed in Section 3.1, inserting a Hadamard transformation within a matrix multiplication can be interpreted as rotating the input or weight space without changing the output distribution. Building upon this, we propose ConvRot, which applies a **group-wise Regular Hadamard Transform (RHT)** to control the scope of rotation and improve both computational efficiency and outlier handling.

Existing rotation-based quantization methods, such as QuaRot and SpinQuant, typically apply a global Hadamard transform of order K , which incurs quadratic complexity $\mathcal{O}(K^2)$ since outliers are redistributed across all channels simultaneously. This becomes prohibitive for large-scale diffusion models. Our key insight is that by partitioning the feature dimension into blocks of size N_0 and applying a **Regular Hadamard Transform** within each block, we can reduce the computational cost and localize outlier redistribution.

Formally, given a standard linear layer

$$\mathbf{Y} = \mathbf{X}\mathbf{W}^\top, \quad \mathbf{X} \in \mathbb{R}^{M \times K}, \mathbf{W} \in \mathbb{R}^{N \times K}, \quad (10)$$

we partition the input and weight matrices into column-wise blocks of size N_0 :

$$\mathbf{X} = [\mathbf{X}_1, \mathbf{X}_2, \dots, \mathbf{X}_{\lceil K/N_0 \rceil}], \quad (11)$$

$$\mathbf{W} = [\mathbf{W}_1, \mathbf{W}_2, \dots, \mathbf{W}_{\lceil K/N_0 \rceil}]. \quad (12)$$

For each block, we insert a Regular Hadamard Rotation

(RHT):

$$\mathbf{Y} = \sum_{i=1}^{\lceil K/N_0 \rceil} \text{RHT}(\mathbf{X}_i) \text{RHT}(\mathbf{W}_i)^\top. \quad (13)$$

By performing group-wise RHT, we reduce computational complexity from $\mathcal{O}(K^2)$ to $\mathcal{O}(K)$, while preserving effective outlier suppression. Importantly, the equivalence property ensures that this local rotation does not change the overall linear transformation; it only redistributes the information within each block, providing finer-grained control over activation distributions. Table 1 shows the Outlier Amplitude, defined as $\max |XH|$ (the maximum absolute value among all elements of XH), under different rotation types and group sizes N_0 .

Existing Hadamard-based quantization methods typically rely on the FWHT implementation from Dao AI Lab [23]. This implementation follows FFT-like butterfly operations and, in its current form, primarily runs on CUDA cores without using Tensor Cores. In our work, we implement ConvRot using matrix multiplication, which reduces additional memory movement and benefits from the optimized matmul pipelines on modern GPUs. This leads to noticeable speedups compared with FWHT-based approaches. Formally, a group rotation of size N_0 can be expressed as a convolution-like operation on the input activation with kernel size $[1, N_0]$, channels equal to N_0 , and stride $(1, N_0)$, which motivates the name **ConvRot** as it integrates the ideas of convolution and rotation.

4.3. ConvLinear4bit

Building on ConvRot, we develop **ConvLinear4bit**, which allows straightforward replacement of original lin-

ear layers for plug-and-play 4-bit inference as shown in Figure 4. ConvLinear4bit integrates ConvRot, quantization, 4-bit matrix multiplication, and dequantization into a single layer.

For ConvRot, we implement the group-wise Hadamard rotation via reshape-based matrix multiplication, minimizing additional memory movement. The quantization, 4-bit matrix multiplication, and dequantization operations follow the design in QuaRot [2] and utilize highly optimized CUDA kernels to take advantage of GPUs’ int4 Tensor Cores.

In summary, ConvRot provides a flexible mechanism to control the number of channels participating in outlier redistribution, trading off computation and smoothing effectiveness. Matmul-based implementation allows leveraging modern GPU pipelines efficiently, while ConvLinear4bit enables practical, plug-and-play 4-bit weight-activation quantization for large-scale diffusion models, achieving significant memory reduction and inference speedup without sacrificing image quality.

5. Experiments

5.1. Setups

Models. We conduct our experiments on FLUX.1-dev and FLUX.1-schnell [3], which are both 12B-parameter text-to-image diffusion models known for their high-quality image generation capabilities. Typically, inference with these models requires over 30GiB of GPU memory, making it hard to deploy on consumer-grade hardware.

Datasets. Following Li et al. [12], we evaluate generation quality on a subset of 5K prompts stratified sampled across categories from the MJHQ-30K dataset [11] and the summarized Densely Captioned Images (sDCI) [29] datasets.

Baselines. We compare ConvRot against three represen-

Table 1. Outlier amplitude after Hadamard rotation across different transformer layers. The two layers respectively represent cases with and without significant row-wise outlier patterns. Additional results are provided in the Appendix 9.1

single_transformer_blocks.0.proj_out						
Hadamard		Outlier Amplitude ↓				
Type		$N_0 = 16$	$N_0 = 64$	$N_0 = 256$	$N_0 = 1024$	Global
Random		6.74-46%	6.47-48%	5.23-58%	3.96-68%	12.43
Standard		6.05-51%	6.48-48%	8.66+20%	16.45+32%	49.59+299%
Regular		6.54-47%	5.57-55%	4.75-62%	3.68-70%	12.43
single_transformer_blocks.0.attn_to_k						
Hadamard		Outlier Amplitude ↓				
Type		$N_0 = 16$	$N_0 = 64$	$N_0 = 256$	$N_0 = 1024$	Global
Random		18.09-57%	12.70-69%	8.59-79%	5.66-86%	41.62
Standard		11.16-73%	6.32-85%	4.29-90%	4.14-90%	4.21-89%
Regular		10.95-74%	6.46-84%	4.48-89%	3.54-92%	41.62

tative baselines: BF16, SVDQuant [12], QuaRot [2], and NF4 [5]. SVDQuant leverages a hybrid 16-bit branch to achieve high-quality 4-bit inference; QuaRot applies rotation-based quantization originally designed for LLMs; and NF4 provides information-theoretically optimal 4-bit quantization primarily for training or LoRA finetuning rather than efficient inference. We provide a detailed comparison of these methods in Appendix 11.

Metrics. We conduct a comprehensive evaluation at both the single-layer and end-to-end levels. For single linear layer analysis, we evaluate **Precision** by measuring the post-rotation outlier amplitude and the maximum layer error. We also assess **Efficiency** by benchmarking the rotation latency and overall layer latency. For the end-to-end text-to-image task, we evaluate from two aspects: **Quality**, using FID [8] (lower is better) and ImageReward (IR) [32] (higher is better); and **Similarity** to the original BF16 model, using LPIPS (lower is better) and PSNR (higher is better). We also report DiT memory footprint and end-to-end generation latency.

5.2. Single-Layer Analysis

Table 1 compares precision and efficiency of different rotation implementations in some single Flux linear layers with the prompt “A cute cat.”. Outlier Amplitude denotes the maximum absolute activation, Rotation Latency the rotation runtime, and Layer Latency the full layer runtime. As shown in Figure 3, layers such as `single_transformer_blocks.{i}.proj_out` and `transformer_blocks.{i}.ff_context.net.2` exhibit pronounced row-wise outliers, with QuaRot’s official Sylvester-type Hadamard (size 15360) reaching Outlier Amplitude 105.63.

Implementation details. For ConvRot, we use per-token/per-channel 4-bit quantization with regular Hadamard rotations, denoting ConvRot- N_0 as group size N_0 . Layers with larger outlier amplitudes use larger rotations ($N_0 = 1024$) to better smooth outliers. SVDQuant and QuaRot use their official defaults. Experiments run on a single RTX 4090 (24GB), with CPU offloading for models exceeding GPU memory.

For the FWHT implementation, small group sizes (e.g., $N_0 = 16$) require many rotation calls, increasing latency, while larger N_0 aggregates row-wise outliers due to the first column of all ones, reducing precision. In contrast, Group-wise RHT shows decreasing Outlier Amplitude with larger N_0 , effectively mitigating row-wise outliers. Rotation latency also decreases with N_0 , reaching 1.246ms at $N_0 = 64$ (1.55× speedup over FP16). Considering both precision and efficiency, we select $N_0 = 256$ as the default settings for ConvRot. For a more detailed performance analysis of FWHT and RHT, please refer to the Appendix 8.

Table 2. End-to-end performance comparison across transformer models. Lower LPIPS/FID and higher PSNR/IR indicate better performance. SVDQuant maintains a parallel 16-bit LoRA branch, while our mixed-precision strategy randomly executes a subset of layers in INT8.

Model	Precision	Method	MJHQ				sDCI			
			Quality		Similarity		Quality		Similarity	
			FID↓	IR↑	LPIPS↓	PSNR↑	FID↓	IR↑	LPIPS↓	PSNR↑
	BF16	–	10.07	0.99	–	–	13.83	1.05	–	–
FLUX.1 -dev (50 Steps)	INT W8A8	Ours	9.81	0.98	0.13	22.62	13.46	1.05	0.15	22.59
	W4A16	NF4	12.10	0.96	0.23	19.23	14.09	0.99	0.24	17.89
	INT W4A4 +16bit LoRA	SVDQuant	10.01	0.97	0.18	20.49	13.71	1.03	0.20	19.65
	INT W4A4	Ours	12.32	0.84	0.22	19.43	16.01	0.87	0.25	17.66
FLUX.1 -schnell (4 Steps)	INT W4A4+20% 8bit Mixed	Ours	10.03	0.97	0.18	20.73	14.00	1.01	0.21	19.41
	BF16	–	11.59	0.91	–	–	11.01	0.97	–	–
	INT W8A8	Ours	10.86	0.96	0.15	21.35	11.09	0.99	0.16	19.91
	W4A16	NF4	11.52	0.91	0.20	18.03	10.93	0.96	0.28	16.77
	INT W4A4 +16bit LoRA	SVDQuant	11.47	0.92	0.21	18.07	10.47	1.02	0.26	19.66
	INT W4A4	Ours	13.38	0.81	0.23	17.5	12.37	0.84	0.30	16.98
	INT W4A4 +20% 8bit Mixed	Ours	11.48	0.92	0.20	18.11	11.13	0.97	0.23	18.71

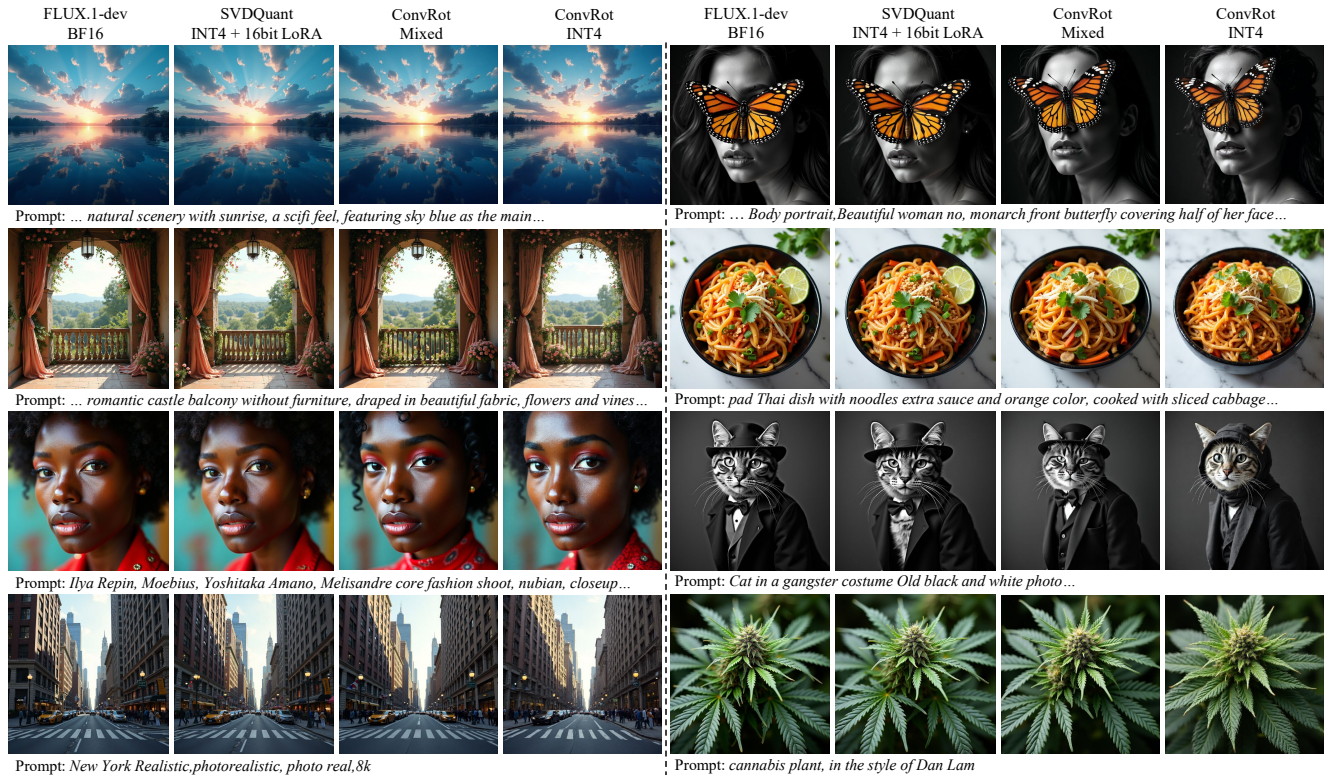


Figure 5. Visual comparison of our method using different rotation sizes on the MJHQ-30K dataset. Prompts cover diverse themes including food, human portraits, animals, landscapes, indoor scenes, and figurines.

5.3. End-to-End Performance on Text-to-Image Generation

We compare our ConvRot approach with SVDQuant and the BF16 baseline on FLUX.1-dev and FLUX.1-Schnell. As

summarized in Table 2, we evaluate both **Similarity** (LPIPS, PSNR) and **Quality** (FID, IR). Lower LPIPS/FID scores and higher PSNR/IR scores indicate better performance.

ConvRot significantly reduces both memory footprint and

Table 3. DiT Memory and Latency comparison on FLUX.1-dev (50 steps) on a single 4090 GPU.

Method	Precision	DiT Memory (GiB)	Latency (s)
Baseline	BF16	22.7	54.6
NF4	W4A16	6.9	38.6
SVDQuant	W4A4 + 16 bit LoRA	6.5	14.9
ConvRot	W4A4	5.6	23.2
	W4A4 + INT8 Mixed	7.0	28.3

latency compared to the BF16 baseline, while introducing only modest degradation in image quality. Metrics such as FID, IR, LPIPS, and PSNR indicate that the quality drop mainly arises from reduced model representation capacity under full INT4 inference, rather than from row-wise outliers. Nevertheless, ConvRot still achieves state-of-the-art visual quality among current INT4 methods, producing images with perceptually acceptable fidelity.

To improve image quality, we adopt a hybrid-precision strategy in which 20% of the layers are empirically selected for INT8 execution, while the rest remain in INT4. Details are provided in Appendix 10. This configuration restores fine-grained details and perceptual quality, closely approaching the performance of SVDQuant with its 16-bit LoRA branch. As shown in Table 2, ConvRot achieves a strong balance between memory efficiency, latency, and image fidelity. Figure 6 illustrates that introducing a fraction of INT8 layers enhances texture sharpness and global coherence compared with full INT4 inference.

5.4. Ablation Study

We further investigate the impact of group size N_0 and rotation type on image generation quality. Unlike the end-to-end experiments in Section 5.3, here we apply the same N_0 uniformly across all layers. This setup isolates the effect



Figure 6. Qualitative impact of hybrid-precision inference on sDCI.

Table 4. Ablation on the choice of precision, rotation type, and size. More results can be found in Table 7.

Precision	Mixed	Rotation		MJHQ			
		Type	Size	FID↓	IR↑	LPIPS↓	PSNR↑
BF16	–	–	–	10.07	0.993	–	–
INT W8A8	Standard	256	9.93	0.981	0.140	22.64	
INT W8A8	Standard	1024	9.91	0.985	0.139	22.61	
INT W8A8	Regular	256	9.82	0.981	0.131	22.62	
INT W8A8	Regular	1024	9.77	0.977	0.129	22.66	
INT W4A4	✓	Standard	Full	98.04	–2.240	0.766	7.70
INT W4A4	✓	Standard	256	12.55	0.835	0.234	19.23
INT W4A4	✓	Standard	1024	13.86	0.808	0.286	18.85
INT W4A4	✓	Standard	256	12.45	0.861	0.193	20.17
INT W4A4	✓	Standard	1024	13.29	0.850	0.290	18.45
INT W4A4	✓	Regular	256	12.32	0.841	0.220	19.43
INT W4A4	✓	Regular	1024	12.30	0.855	0.215	19.52
INT W4A4	✓	Regular	256	10.03	0.973	0.186	20.73
INT W4A4	✓	Regular	1024	10.02	0.983	0.184	20.71

of rotation configuration on the model’s representational capacity and image fidelity.

More ablation results are provided in the Table 7.

6. Conclusion

We present ConvRot, a novel rotation-based quantization framework for diffusion transformers that enables efficient W4A4 INT4 inference while preserving image quality. To address the challenges of row-wise and column-wise outliers in activations, we introduce a group-wise rotation scheme based on regular Hadamard matrices, reducing computational complexity from quadratic to linear and significantly lowering rotation latency compared to global rotations. Building on this, we design ConvLinear4bit, a plug-and-play module that fuses rotation, quantization, GEMM, and dequantization, allowing all linear layers in a diffusion model to be quantized without retraining. Extensive experiments on FLUX.1-dev demonstrate that our approach stably suppresses outliers, reduces memory usage by $4.05\times$, and achieves a $2.26\times$ speedup, while maintaining high-fidelity image generation. To our knowledge, this work is the first to apply rotation-based quantization to diffusion transformers for fully INT4 W4A4 inference, providing a practical solution for accelerating large-scale text-to-image generation with minimal quality loss.

References

- [1] Krish Agarwal, Rishi Astra, Adnan Hoque, Mudhakar Srivatsa, Raghu Ganti, Less Wright, and Sijia Chen. Hadacore: Tensor core accelerated hadamard transform kernel. *arXiv preprint arXiv:2412.08832*, 2024. 1
- [2] Saleh Ashkboos, Amirkeivan Mohtashami, Maximilian Croci, Bo Li, Pashmina Cameron, Martin Jaggi, Dan Alistarh, Torsten Hoefer, and James Hensman. Quarot: Outlier-free 4-bit inference in rotated llms. *NeurIPS*, 2024. 1, 2, 4, 6, 3
- [3] Black-Forest-Labs. Flux.1, 2024. 1, 6
- [4] Tim Dettmers, Mike Lewis, Younes Belkada, and Luke Zettle-

moyer. Gpt3. int8 (): 8-bit matrix multiplication for transformers at scale. *NeurIPS*, 2022. 1, 2

[5] Tim Dettmers, Artidoro Pagnoni, Ari Holtzman, and Luke Zettlemoyer. QLoRA: Efficient finetuning of quantized LLMs. In *NeurIPS*, 2023. 3, 6, 4

[6] Marco Federici, Riccardo Del Chiaro, Boris van Breugel, Paul Whatmough, and Markus Nagel. Hadanorm: Diffusion transformer quantization through mean-centered transformations. *arXiv preprint arXiv:2506.09932*, 2025. 2, 5

[7] Elias Frantar, Saleh Ashkboos, Torsten Hoefer, and Dan Alistarh. GPTQ: Accurate post-training compression for generative pretrained transformers. *ICLR*, 2023. 2

[8] Martin Heusel, Hubert Ramsauer, Thomas Unterthiner, Bernhard Nessler, and Sepp Hochreiter. Gans trained by a two time-scale update rule converge to a local nash equilibrium. *NeurIPS*, 2017. 6

[9] Jonathan Ho, Ajay Jain, and Pieter Abbeel. Denoising diffusion probabilistic models. *NeurIPS*, 2020. 1, 2

[10] Weijie Kong, Qi Tian, Zijian Zhang, Rox Min, Zuozhuo Dai, Jin Zhou, Jiangfeng Xiong, Xin Li, Bo Wu, Jianwei Zhang, et al. Hunyuanyvideo: A systematic framework for large video generative models. *arXiv preprint arXiv:2412.03603*, 2024. 2

[11] Daiqing Li, Aleks Kamko, Ehsan Akhgari, Ali Sabet, Linmiao Xu, and Suhail Doshi. Playground v2.5: Three insights towards enhancing aesthetic quality in text-to-image generation, 2024. 6

[12] Muyang Li, Yujun Lin, Zhekai Zhang, Tianle Cai, Xiuyu Li, Junxian Guo, Enze Xie, Chenlin Meng, Jun-Yan Zhu, and Song Han. Svdquant: Absorbing outliers by low-rank components for 4-bit diffusion models. *arXiv preprint arXiv:2411.05007*, 2024. 3, 6, 4

[13] Xiuyu Li, Yijiang Liu, Long Lian, Huanrui Yang, Zhen Dong, Daniel Kang, Shanghang Zhang, and Kurt Keutzer. Q-diffusion: Quantizing diffusion models. In *ICCV*, 2023. 3

[14] Haokun Lin, Haobo Xu, Yichen Wu, Jingzhi Cui, Yingtao Zhang, Linzhan Mou, Linqi Song, Zhenan Sun, and Ying Wei. Duquant: Distributing outliers via dual transformation makes stronger quantized llms. *Advances in Neural Information Processing Systems*, 37:87766–87800, 2024. 1, 2, 4

[15] Ji Lin, Jiaming Tang, Haotian Tang, Shang Yang, Wei-Ming Chen, Wei-Chen Wang, Guangxuan Xiao, Xingyu Dang, Chuang Gan, and Song Han. Awq: Activation-aware weight quantization for on-device llm compression and acceleration. In *MLSys*, 2024. 2

[16] Feng Liu, Shiwei Zhang, Xiaofeng Wang, Yujie Wei, Haonan Qiu, Yuzhong Zhao, Yingya Zhang, Qixiang Ye, and Fang Wan. Timestep embedding tells: It's time to cache for video diffusion model. In *Proceedings of the Computer Vision and Pattern Recognition Conference*, pages 7353–7363, 2025. 3

[17] Zechun Liu, Changsheng Zhao, Igor Fedorov, Bilge Soran, Dhruv Choudhary, Raghuraman Krishnamoorthi, Vikas Chandra, Yuandong Tian, and Tijmen Blankevoort. Spinquant–llm quantization with learned rotations. *arXiv preprint arXiv:2405.16406*, 2024. 1, 2, 3, 4

[18] Cheng Lu, Yuhao Zhou, Fan Bao, Jianfei Chen, Chongxuan Li, and Jun Zhu. Dpm-solver: A fast ode solver for diffusion probabilistic model sampling in around 10 steps. In *NeurIPS*, 2022. 3

[19] Cheng Lu, Yuhao Zhou, Fan Bao, Jianfei Chen, Chongxuan Li, and Jun Zhu. Dpm-solver++: Fast solver for guided sampling of diffusion probabilistic models. *arXiv preprint arXiv:2211.01095*, 2022. 3

[20] Simian Luo, Yiqin Tan, Longbo Huang, Jian Li, and Hang Zhao. Latent consistency models: Synthesizing high-resolution images with few-step inference. *arXiv preprint arXiv: 2310.04378*, 2023. 3

[21] Jiri Matousek. *Geometric discrepancy: An illustrated guide*. Springer Science & Business Media, 1999. 4

[22] William Peebles and Saining Xie. Scalable diffusion models with transformers. In *ICCV*, 2023. 1, 2

[23] Amit Portnoy. hadamard–transform: Fast walsh–hadamard transform (fwht) implementation in pytorch. [https://pypi.org/project/hadamard–transform/](https://pypi.org/project/hadamard-transform/), 2022. Version 0.1.3, released July 5, 2022. 5, 1

[24] Robin Rombach, Andreas Blattmann, Dominik Lorenz, Patrick Esser, and Björn Ommer. High-resolution image synthesis with latent diffusion models. In *CVPR*, 2022. 1

[25] Tim Salimans and Jonathan Ho. Progressive distillation for fast sampling of diffusion models. In *ICLR*, 2021. 3

[26] Jiaming Song, Chenlin Meng, and Stefano Ermon. Denoising diffusion implicit models. In *ICLR*, 2020. 3

[27] Joel Spencer. Six standard deviations suffice. *Transactions of the American mathematical society*, 289(2):679–706, 1985. 4

[28] Albert Tseng, Jerry Chee, Qingyao Sun, Volodymyr Kuleshov, and Christopher De Sa. Quip#: Even better llm quantization with hadamard incoherence and lattice codebooks. *arXiv preprint arXiv:2402.04396*, 2024. 1, 2, 3

[29] Jack Urbanek, Florian Bordes, Pietro Astolfi, Mary Williamson, Vasu Sharma, and Adriana Romero-Soriano. A picture is worth more than 77 text tokens: Evaluating clip-style models on dense captions. In *CVPR*, 2024. 6

[30] Chenfei Wu, Jiahao Li, Jingren Zhou, Junyang Lin, Kaiyuan Gao, Kun Yan, Sheng-ming Yin, Shuai Bai, Xiao Xu, Yilei Chen, et al. Qwen-image technical report. *arXiv preprint arXiv:2508.02324*, 2025. 1, 2

[31] Guangxuan Xiao, Ji Lin, Mickael Seznec, Hao Wu, Julien Demouth, and Song Han. Smoothquant: Accurate and efficient post-training quantization for large language models. In *ICML*, 2023. 1, 2

[32] Jiazheng Xu, Xiao Liu, Yuchen Wu, Yuxuan Tong, Qinkai Li, Ming Ding, Jie Tang, and Yuxiao Dong. Imagereward: Learning and evaluating human preferences for text-to-image generation. *NeurIPS*, 2024. 6

[33] Tianwei Yin, Michaël Gharbi, Richard Zhang, Eli Shechtman, Fredo Durand, William T Freeman, and Taesung Park. One-step diffusion with distribution matching distillation. In *CVPR*, 2024. 3

[34] Tianchen Zhao, Tongcheng Fang, Enshu Liu, Wan Rui, Widayadewi Soedarmadjie, Shiyao Li, Zinan Lin, Guohao Dai, Shengen Yan, Huazhong Yang, et al. Vudit-q: Efficient and accurate quantization of diffusion transformers for image and video generation. *arXiv preprint arXiv:2406.02540*, 2024. 3

[35] Tianchen Zhao, Xuefei Ning, Tongcheng Fang, Enshu Liu, Guyue Huang, Zinan Lin, Shengen Yan, Guohao Dai, and Yu

Wang. Mixdq: Memory-efficient few-step text-to-image diffusion models with metric-decoupled mixed precision quantization. In *ECCV*, 2024. [3](#)

[36] Wangbo Zhao, Yizeng Han, Jiasheng Tang, Kai Wang, Yibing Song, Gao Huang, Fan Wang, and Yang You. Dynamic diffusion transformer. *arXiv preprint arXiv:2410.03456*, 2024. [3](#)

[37] Xunyu Zhu, Jian Li, Yong Liu, Can Ma, and Weiping Wang. A survey on model compression for large language models. *Transactions of the Association for Computational Linguistics*, 12:1556–1577, 2024. [1](#)

ConvRot: Rotation-Based Plug-and-Play 4-bit Quantization for Diffusion Transformers

Supplementary Material

7. Proofs

7.1. Proof of Theorem 3.1 (Column Sum Squared Property)

Proof. Let \mathbf{H}_n be a Hadamard matrix of order n , satisfying $\mathbf{H}_n \mathbf{H}_n^\top = n \mathbf{I}_n$. Define the column sums as $c_j = \sum_{i=1}^n H_{ij}$ for $j = 1, \dots, n$. We consider the squared ℓ_2 norm of the vector of column sums:

$$\sum_{j=1}^n c_j^2 = \sum_{j=1}^n \left(\sum_{i=1}^n H_{ij} \right)^2. \quad (14)$$

This can be expressed as

$$\sum_{j=1}^n c_j^2 = \|\mathbf{H}_n^\top \mathbf{1}\|_2^2 = \mathbf{1}^\top \mathbf{H}_n \mathbf{H}_n^\top \mathbf{1}. \quad (15)$$

Using the orthogonality property $\mathbf{H}_n \mathbf{H}_n^\top = n \mathbf{I}_n$, we obtain

$$\mathbf{1}^\top \mathbf{H}_n \mathbf{H}_n^\top \mathbf{1} = n \cdot \mathbf{1}^\top \mathbf{1} = n \cdot n = n^2. \quad (16)$$

Therefore,

$$\sum_{j=1}^n \left(\sum_{i=1}^n H_{ij} \right)^2 = n^2, \quad (17)$$

which proves the claim. \square

7.2. Proof of Theorem 3.2 (Column Discrepancy of Regular Hadamard)

Proof. By definition, the column discrepancy of \mathbf{H}_n is

$$\|\mathbf{H}_n^\top \mathbf{1}\|_\infty = \max_{1 \leq j \leq n} \left| \sum_{i=1}^n H_{ij} \right|. \quad (18)$$

From Appendix 7.1, we know that the squared column sums satisfy

$$\sum_{j=1}^n \left(\sum_{i=1}^n H_{ij} \right)^2 = n^2. \quad (19)$$

If \mathbf{H}_n is regular, each column sum satisfies $\sum_i H_{ij} = \pm \sqrt{n}$, so the maximum absolute column sum is exactly \sqrt{n} . Since \sqrt{n} is also the theoretical minimum discrepancy achievable by any Hadamard matrix, regular Hadamard matrices attain the optimum. \square

7.3. Proof of Theorem 3.3 (Kronecker Construction of Regular Hadamard Matrices)

Proof. We prove by induction on k .

Base case: For $k = 1$, the given 4×4 matrix \mathbf{H}_4 is regular, since each row and column sums to $\pm 2 = \pm \sqrt{4}$.

Inductive step: Assume \mathbf{H}_{4^k} is a regular Hadamard matrix, i.e., each row and column sums to $\pm \sqrt{4^k}$. Consider $\mathbf{H}_{4^{k+1}} = \mathbf{H}_{4^k} \otimes \mathbf{H}_4$. For any column of $\mathbf{H}_{4^{k+1}}$, the Kronecker product structure ensures that its entries are composed of four blocks, each proportional to a column of \mathbf{H}_{4^k} . Therefore, the column sum is

$$\sum_i H_{ij}^{(4^{k+1})} = \left(\sum_u H_{u,v}^{(4^k)} \right) \cdot \left(\sum_w H_{w,z}^{(4)} \right), \quad (20)$$

where v, z index the corresponding columns in \mathbf{H}_{4^k} and \mathbf{H}_4 . By the induction hypothesis, $\sum_u H_{u,v}^{(4^k)} = \pm \sqrt{4^k}$, and since \mathbf{H}_4 is regular, $\sum_w H_{w,z}^{(4)} = \pm 2$. Thus,

$$\sum_i H_{ij}^{(4^{k+1})} = (\pm \sqrt{4^k})(\pm 2) = \pm \sqrt{4^{k+1}}. \quad (21)$$

Hence $\mathbf{H}_{4^{k+1}}$ is also regular. By induction, a regular Hadamard matrix exists for all $n = 4^k$. \square

8. Efficiency Analysis

In this section, we compare the efficiency of the FWHT implementation from Dao AI Lab [23] with our proposed group-wise RHT.* It is worth noting that the butterfly operations in FWHT correspond to the Sylvester-type Hadamard transform, which restricts FWHT from being applied to modified Hadamard matrices.

From a theoretical perspective, applying a global Hadamard transform directly via matrix multiplication incurs a quadratic cost of $\mathcal{O}(K^2)$ when the number of channels is K . QuaRot [2] decomposes K as $K = 2^n m$, where the 2^n part can be accelerated using FWHT with complexity $\mathcal{O}(Kn)$, giving an overall complexity of $\mathcal{O}(K(m+n))$. From an engineering standpoint, however, the widely used FWHT implementation from Dao AI Lab relies on FFT-like butterfly operators and does not utilize Tensor Cores. While butterfly operations can in principle be reformulated into small matrix multiplications to make use of Tensor Core acceleration [1], this optimization has not yet seen broad

*For some reason, the experiments in this section were conducted on an A100 GPU, rather than the RTX 4090 used in the main paper.

Table 5. Profiling statistics of FWHT kernels with different group sizes (Rotation Latency).

Group Size	Shared Mem	Blocks/SM	Warps/SM	Occupancy	Wall Dur. (ms)
64	256	10240	2560	13%	0.822
256	1024	2560	2560	50%	0.209
1024	4096	640	2560	100%	0.229

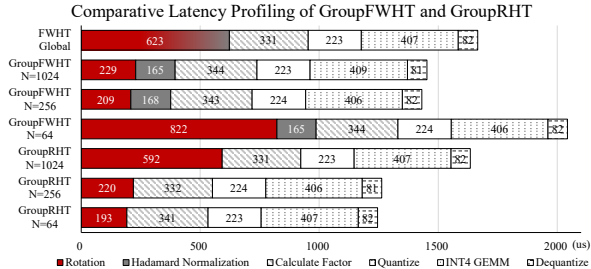


Figure 7. Latency comparison of FWHT and RHT under different group sizes.

adoption in existing methods, so we do not include its performance in our comparisons.

Although ConvLinear4bit integrates rotation, quantization, INT4 GEMM, and dequantization into a unified module, we do not fuse these operations at the kernel level. Instead, all stages directly reuse the existing implementations from QuaRot [2]. As shown in Figure 7, we benchmark both FWHT and RHT under group sizes of 64, 256, and 1024 using a linear layer with $W \in \mathbb{R}^{3072 \times 15360}$, $X \in \mathbb{R}^{1 \times 4608 \times 15360}$, and $Y \in \mathbb{R}^{1 \times 4608 \times 3072}$. The only performance difference between the two methods comes from the rotation stage. Because FWHT cannot parallelize the normalization step ($1/\sqrt{n}$), an additional Hadamard normalization must be applied, further increasing its latency. For the global FWHT case, since the size 15360 does not appear in QuaRot’s precomputed Hadamard list, the transform must be implemented by combining FWHT with matrix multiplication; both this matmul and the subsequent normalization are executed using FP16 GEMM kernels, and we report their combined latency.

As shown in Table 5, FWHT exhibits poor hardware utilization when the group size is small. Similarly, group-wise RHT also suffers from low occupancy at a group size of 64, but achieves strong performance at the more commonly used group sizes of 256 and 1024. Although group-wise RHT becomes slightly slower than FWHT at a group size of 1024 due to its larger computational load, this gap can be reduced with further kernel optimization, which is beyond the scope of this paper and left for future work.

9. More Experiment Results

In this section, we present additional experimental results. At the layer level, we show the outlier suppression effect of

different Hadamard matrices and group-wise rotations across various linear layers in FLUX.1-dev, demonstrating the effectiveness of ConvRot. At the end-to-end level, we evaluate the impact of different Hadamard matrices, group-wise rotations, and quantization bitwidths on the final generated image quality.

9.1. Layer-level Outlier Suppression Analysis

As shown in Table 6, we provide a detailed comparison of three Hadamard matrices and four group sizes across different layers in FLUX.1-dev, using the prompt “a cute cat”. The results indicate that, in general, larger group sizes N lead to stronger outlier suppression. The Regular matrix exhibits the most stable performance, while the Standard matrix may fail in layers with row-wise outliers, such as `single_transformer_blocks_{i}.proj_out`.

9.2. End-to-End Image Generation Ablation

As shown in Table 7, we compare the end-to-end generation quality obtained using the Regular Hadamard matrix versus the Standard Hadamard matrix. To evaluate the effect of block size, we modify QuaRot by replacing its standard full-rank FWHT with a block-wise FWHT, denoted as QuaRot[†]. The results show that under the W4A4 setting, QuaRot with a global Standard Hadamard transform completely fails. Under local block-wise settings, using the Regular Hadamard matrix yields noticeably better performance than using the Standard version, whereas the gap becomes less pronounced in the W8A8 setting due to the reduced difficulty of 8-bit quantization. These findings indicate that simply adopting a block-wise strategy already mitigates much of the outlier concentration effect caused by the Standard Hadamard matrix, while switching to the Regular matrix eliminates this issue entirely. It is worth noting that we do not evaluate a global RHT, as there is currently no known construction method for Regular matrices of arbitrary sizes. Our proposed construction Theorem 3.3 only applies to sizes that are powers of four, and therefore can be used only for group-wise local transforms rather than global ones.

As shown in Figure 9, we evaluate the impact of quantization bitwidth on end-to-end image generation quality. By default, ConvRot quantizes all linear layers in the (single) transformer blocks, except for `transformer_blocks_18_ff_context_net_2`, `transformer_blocks_18_ff_net_2` and `single_transformer_blocks.37.proj_out`[†].

Under the W8A8 setting, ConvRot achieves good image quality. Under W4A4, ConvRot exhibits the best inference speed with a moderate and acceptable degradation in image

[†]These layers are the final layers of the `transformer_blocks` and `single_transformer_blocks`, which significantly affect image quality. Experiments show that keeping them at higher precision has minimal impact on model speed after quantization.

Table 6. Outlier amplitude after rotation across transformer layers in FLUX.1-dev. **Bold** and underlined numbers indicate the largest and second-largest reduction (i.e., the strongest suppression effect).

single_transformer_blocks_0_attn_to_k						
Hadamard		Outlier Amplitude ↓				
Type		$N_0 = 16$	$N_0 = 64$	$N_0 = 256$	$N_0 = 1024$	Global
Random		18.09- 57%	12.70- 69%	8.59- 79%	5.66- 86%	41.62
Standard		11.16- 73%	6.32- 85%	4.29- 90%	4.14- 90%	41.62
Regular		10.95- 74%	6.46- 84%	4.48- 89%	3.54 - 92%	41.62
single_transformer_blocks_27_proj_mlp						
Type		$N_0 = 16$	$N_0 = 64$	$N_0 = 256$	$N_0 = 1024$	Global
Random		6.84- 43%	3.71- 69%	3.00- 75%	1.97- 84%	12.11
Standard		3.70- 69%	2.42- 80%	<u>1.91</u> - 84%	2.12- 82%	1.78 - 85%
Regular		3.68- 70%	2.42- 80%	2.35- 81%	2.04- 83%	12.11
single_transformer_blocks_24_proj_out						
Type		$N_0 = 16$	$N_0 = 64$	$N_0 = 256$	$N_0 = 1024$	Global
Random		3.57- 53%	2.88- 62%	2.43- 68%	2.14 - 72%	7.59
Standard		3.27- 57%	3.88- 49%	6.45- 15%	10.79+ 42%	30.97+ 308%
Regular		3.19- 58%	3.54- 53%	2.70- 64%	2.25 - 70%	7.59
transformer_blocks_12_ff_context_net_2						
Type		$N_0 = 16$	$N_0 = 64$	$N_0 = 256$	$N_0 = 1024$	Global
Random		16.94- 27%	14.25- 38%	10.38- 55%	<u>9.52</u> - 59%	23.11
Standard		13.23- 43%	10.60- 54%	12.70- 45%	20.39- 12%	43.81+ 90%
Regular		13.23- 43%	10.65- 54%	8.99 - 61%	9.74- 58%	23.11
transformer_blocks_3_attn_to_out_0						
Type		$N_0 = 16$	$N_0 = 64$	$N_0 = 256$	$N_0 = 1024$	Global
Random		6.56+ 2%	5.65- 12%	4.96- 23%	2.79- 57%	6.45
Standard		6.87+ 7%	6.05- 6%	4.06- 37%	2.75- 57%	2.41 - 63%
Regular		5.57- 14%	6.76+ 5%	4.38- 32%	2.51 - 61%	6.45
transformer_blocks_2_ff_net_2						
Type		$N_0 = 16$	$N_0 = 64$	$N_0 = 256$	$N_0 = 1024$	Global
Random		1.96- 37%	1.27- 59%	1.02- 67%	<u>0.94</u> - 70%	3.10
Standard		1.28- 59%	1.22- 61%	1.36- 56%	2.15- 30%	4.94+ 60%
Regular		1.17- 62%	0.99- 68%	0.94 - 70%	1.00- 68%	3.10

quality. By applying a mixed-precision strategy, using 8-bit mixed precision for 20% of sensitive layer, the degradation can be effectively mitigated, improving overall image quality. Details of the mixed-precision strategy can be found in Appendix 10.

Figure 8 further illustrates the degradation pattern observed under W4A4. Although high-frequency details such as clothing wrinkles and hair are preserved, low-frequency regions exhibit noticeable mosaicking. We rule out the influ-

ence of outlier suppression, since restoring selected sensitive layers to int8 recovers low-frequency details, even though these layers do not exhibit significant outlier activations (e.g., `transformer_blocks_{i}_attn_to_out_0`).

We hypothesize that this is due to the limited representational range of 4-bit quantization, which makes it difficult for the model to capture subtle transitions. Such degradation commonly occurs in smooth regions, such as skies or walls.



Figure 8. Visualization of image degradation under low-bit quantization.

10. Mixed-Precision Strategy

As shown in Figure 8, we observe noticeable image degradation under the W4A4 setting. We hypothesize that the loss of low-frequency details arises from the limited representational capacity of W4A4, which struggles to capture subtle transitions. To compensate for this deficiency, we introduce additional expressiveness into the quantized model.

Inspired by the 16-bit LoRA used in SVDQuant, we adopt a mixed-precision strategy: based on empirical observations, we manually quantize layers one by one and find that a subset of layers has a disproportionately large impact on image quality. These layers are therefore assigned higher precision (W8A8 instead of W4A4) to improve overall fidelity rather than being kept in FP16/BF16. Notably, during this process we did not observe strong outlier activations in these sensitive layers, suggesting that their importance is tied more to their functional role in the network than to activation statistics.

In practice, we select approximately 20% of the linear layers for W8A8 quantization; the exact layer list is provided in Table 8.

11. Comparison with Existing Quantization Methods

Comparison with QuaRot. QuaRot [2] is a calibration-free PTQ method designed for LLMs, reducing rotation overhead by fusing rotations into weights and accelerating them via FWHT. However, its rotation-reduction strategy does not apply to DiT, and the FWHT induces row-wise outlier aggregation. Building upon QuaRot, we retain its quantization, INT4 GEMM, and dequantization kernels while introducing our Group RHT within a unified ConvLinear4bit layer.

Table 7. Ablation on the choice of rotation type and size. We compare Standard and Regular Hadamard transforms under global and block-wise settings across different quantization precisions. Mixed refers to the use of a mixed precision strategy, where approximately 20% of the linear layers are quantized to INT 8.

Model	Precision	Mixed	Rotation		MJHQ				sDCI			
			Type	Size	FID↓	IR↑	LPIPS↓	PSNR↑	FID↓	IR↑	LPIPS↓	PSNR↑
FLUX.1 -dev (50 Steps)	BF16	–	–	–	10.07	0.993	–	–	13.84	1.055	–	–
	INT W8A8	Standard	256	9.93	0.981	0.140	22.64	13.45	1.018	0.157	22.60	
	INT W8A8	Standard	1024	9.91	0.985	0.139	22.61	13.50	1.001	0.166	22.69	
	INT W8A8	Regular	256	9.82	0.981	0.131	22.62	13.47	1.050	0.157	22.59	
	INT W8A8	Regular	1024	9.77	0.977	0.129	22.66	13.46	1.044	0.148	22.62	
	INT W4A4	✓	Standard	Full	98.04	-2.240	0.766	7.70	110.84	-2.277	0.767	7.41
	INT W4A4	Standard	256	12.55	0.835	0.234	19.23	14.09	0.994	0.247	17.89	
	INT W4A4	Standard	1024	13.86	0.808	0.286	18.85	16.99	0.913	0.345	16.83	
	INT W4A4	✓	Standard	256	12.45	0.861	0.193	20.17	15.86	0.878	0.241	19.24
	INT W4A4	✓	Standard	1024	13.29	0.850	0.290	18.45	16.53	0.900	0.360	16.22
FLUX.1 -schnell (50 Steps)	INT W4A4	Regular	256	12.32	0.841	0.220	19.43	16.02	0.870	0.249	17.66	
	INT W4A4	Regular	1024	12.30	0.855	0.215	19.52	15.87	0.880	0.245	17.72	
	INT W4A4	✓	Regular	256	10.03	0.973	0.186	20.73	14.00	1.020	0.214	19.41
	INT W4A4	✓	Regular	1024	10.02	0.983	0.184	20.71	14.02	1.020	0.224	19.42
	BF16	–	–	–	11.59	0.915	–	–	11.01	0.974	–	–
	INT W8A8	Standard	256	10.90	0.962	0.151	21.36	11.28	1.006	0.152	19.93	
	INT W8A8	Standard	1024	10.88	0.971	0.142	21.68	11.25	1.002	0.155	20.15	
	INT W8A8	Regular	256	10.86	0.958	0.151	21.36	11.09	0.995	0.157	19.91	
	INT W8A8	Regular	1024	10.84	0.965	0.151	21.39	11.05	1.007	0.136	20.11	
	INT W4A4	✓	Standard	Full	101.09	-2.252	0.811	6.54	114.01	-2.279	0.601	6.75
FLUX.1 -schnell (50 Steps)	INT W4A4	Standard	256	14.47	0.803	0.242	17.59	13.54	0.894	0.313	16.88	
	INT W4A4	Standard	1024	16.19	0.761	0.259	16.44	13.86	0.910	0.353	16.47	
	INT W4A4	✓	Standard	256	12.13	0.883	0.204	18.05	12.41	0.965	0.281	18.66
	INT W4A4	✓	Standard	1024	14.07	0.890	0.290	16.74	13.22	0.970	0.270	17.80
	INT W4A4	Regular	256	13.38	0.814	0.231	17.50	12.37	0.844	0.301	16.98	
	INT W4A4	Regular	1024	12.88	0.868	0.224	17.73	13.59	0.949	0.314	16.92	
	INT W4A4	✓	Regular	256	11.49	0.926	0.201	18.11	11.13	0.975	0.228	18.71
	INT W4A4	✓	Regular	1024	11.27	0.909	0.203	18.06	11.31	0.995	0.245	18.68

Group-wise rotation lowers computational cost and mitigates DiT’s outlier amplification, and the use of regular Hadamard matrices eliminates the amplification issue entirely.

Comparison with NF4. NF4 [5] is the 4-bit NormalFloat data type introduced in QLoRA, designed to be information-theoretically optimal for normally distributed weights and effective for low-precision finetuning. However, NF4 requires dequantization into higher-precision formats during computation and therefore provides limited inference-time acceleration when applied to diffusion transformers. In con-

trast, our ConvRot method enables direct INT4 computation with integrated rotation and quantization, achieving significant speedups during inference.

Comparison with DuQuant. DuQuant [14] also explores block-wise rotation for LLMs, targeting massive activations by permuting affected channels and applying standard Hadamard transforms inside each block. Its complex matrix construction (SmoothQuant + permutation + two rotations), however, offers limited speed benefits. In contrast, our Group RHT is tailored to DiT’s row-wise outlier structure, avoids heavy matrix design, and enables a substantially faster rotation procedure.

Comparison with SVDQuant. SVDQuant [12] is the first to achieve W4A4 quantization on DiT, delivering strong image quality and impressive speed through comprehensive engineering optimizations. We highly appreciate the authors’ engagement with the open-source community, its out-of-the-box usability makes reproduction and comparison straightforward. However, its reliance on the specialized nunchaku inference engine restricts broader applicability. In contrast, our method is lightweight and easy to integrate, requires no

Table 8. Layer-wise mixed-precision quantization list.

Layer	Precision
transformer_blocks_{i}.attn_to_out_0	W8A8
single_transformer_blocks_{i}.attn_to_v	W8A8
single_transformer_blocks_37.proj_out	W8A8
transformer_blocks_18_ff_context_net_2	W8A8
transformer_blocks_18_ff_net_2	W8A8
others	W4A4

additional runtime dependencies, and supports plug-and-play DiT quantization with competitive performance.

Comparison with HadaNorm. HadaNorm [6] attributes the failure of standard Hadamard transforms to mean and scale differences across channels, where the all-ones row prevents non-zero-mean channels from avoiding long-tailed activations; they address this via explicit mean subtraction. Our approach resolves the issue directly through rotation-matrix design, eliminating extra steps. As HadaNorm is not yet open-sourced and reports limited experiments, we omit a direct comparison. Incidentally, we were unaware of this work when developing our method; after arriving at our approach independently, we were pleased to find that other researchers had identified a similar problem and proposed an alternative, effective solution.

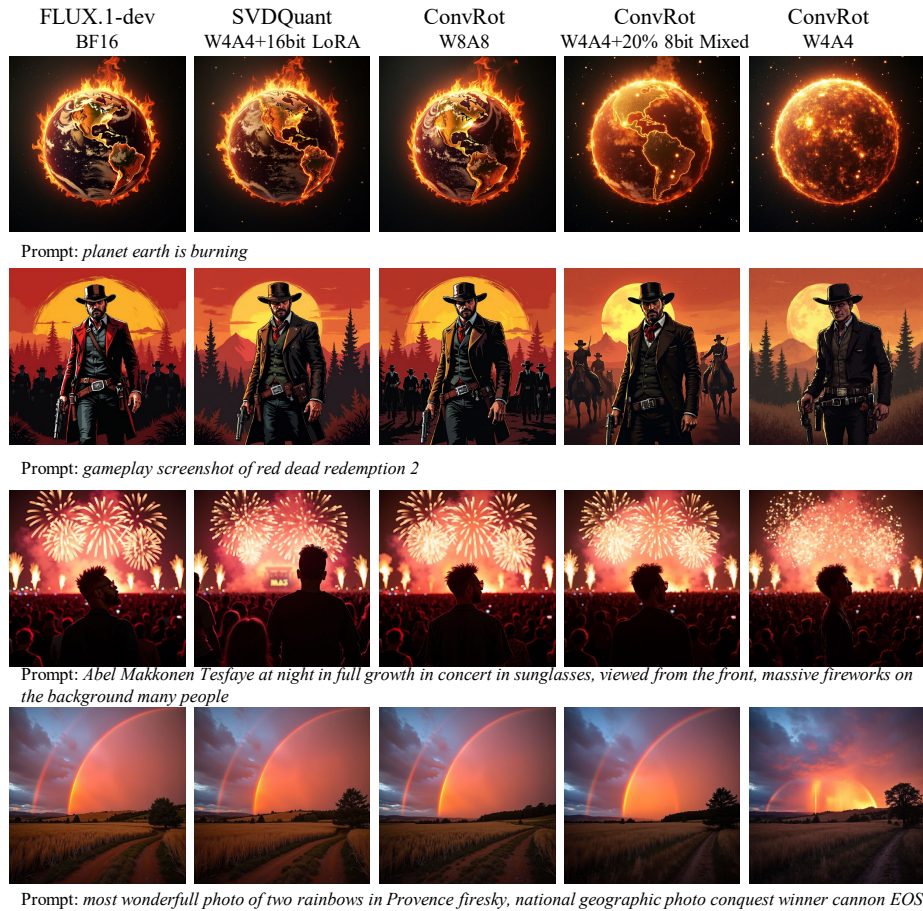


Figure 9. Ablation study on the impact of quantization bitwidth on end-to-end image generation quality.